European Journal of Mechanics / A Solids 106 (2024) 105323

Contents lists available at ScienceDirect

European Journal of Mechanics / A Solids

journal homepage: www.elsevier.com/locate/ejmsol

Full Length Article

Mechanics of polymers obtained by layered photopolymerization

Roberto Brighenti [a,*], Mattia P. Cosma [b], Silvia Monchetti [a]

[a] Department of Civil & Environmental Engineering, University of Florence, Via di S. Marta 3, 50199, Florence, Italy
[b] Department of Engineering and Architecture, University of Parma, Parco Area delle Scienze 181/A, 43124, Parma, Italy

ARTICLE INFO

Keywords:
Polymers
Photo-induced polymerization
Additive Manufacturing
Layered photopolymerization
Mechanical response

ABSTRACT

The photopolymerization process is a high-precision and efficient technology to obtain solid polymers starting from a photosensible liquid resin made of monomer units. This technology is widely used in Additive Manufacturing (AM) to produce objects whose size can fall within the range $10^{-5} - 10^{0}$ m. The outstanding potentialities of this technology can be harnessed to tailor the structure of a polymeric material by controlling how the light-induced polymerization process is performed, typically by operating on subsequent layers forming the final object. The present research illustrates the chemical-physics phenomena involved in the photo-polymerization and presents a multi-physics framework and the related governing equations. Its implementation within a computational framework is developed and several simulations demonstrating the influence of the AM printing setup on the final microstructure of the obtained polymer are presented. It is shown that photopolymerization-based AM technology allows us to finely tune the mechanical properties distribution within the material domain, enabling the material's architecture to be tailored to the application of interest.

1. Introduction

Visible or ultraviolet (UV) light can be effectively used to trigger and propagate a polymerization reaction in photopolymers in order to a solid structure. A photopolymer, or light-activated resin, can be obtained starting from a liquid resin by exploiting the light-activation capability of cromophores (photoinitiators) embedded in the monomer liquid domain exposed to light with a suitable wavelength. The solid polymer forms because of the microstructure evolution due to the cross-linking mechanism taking place between the monomer units and the emerging chains to form a linear or cross-linked structure, a process usually referred to as curing (Phillips, 1984; Yamaguchi and Nakamoto, 1998; Bowman et al., 2008; Chen et al., 2016; Bikas et al., 2016; Al Rashid et al., 2021).

A so-called photopolymer is made of a mixture of monomers and oligomers which can polymerize in the presence of light, resulting in a thermoset polymer. Photo-curing is usually obtained by using high-energy light sources, such as lasers; however, visible light can also be used. Most of the photopolymers are not readily activated by light, and the presence of a photoinitiator is usually required. Photoinitiators are compounds that exposed to light decompose into reactive species which activate the polymerization induced by functional groups on the oligomers.

The final structural and chemical properties of the photopolymerized material can be easily controlled within the domain of interest by properly setting the proportions of monomers and oligomers composing the photopolymer.

The photopolymerization mechanism is nowadays effectively implemented in advanced Additive Manufacturing (AM) technologies (Andrzejewska and Grajek, 2017; Schwartz, 2022; Long et al., 2009; Brighenti et al., 2021a, 2021b) (such as Stereolithography (SLA), Digital light processing (DLP), etc.), enabling to obtain high-precision parts – whose size can fall in a wide range of dimensions, roughly $10^{-5} - 10^{0}$ m – suitable to be used in medicine, nanotechnology applications, fabrication of small-scale metamaterials, energy and advanced technological applications (optoelectronics, holographic data storage, …), etc. (Andrzejewska and Grajek, 2017; Schwartz, 2022; Han et al., 2019; Bella and Bongiovanni, 2013; Buss et al., 2018).

Photopolymerization technology offers new and unprecedented possibilities of controlling the physical and mechanical material properties within the printing domain, enabling a space-time tuning; this allows us to obtain the so-called architected materials, whose behavior at the macroscale can be controlled through their microstructure (Brighenti et al., 2021c).

Some studies have considered modelling the photopolymerization process by accounting for the main physical phenomena involved (Westbeek et al., 2018, 2020; Classens et al., 2021); in particular, the

* Corresponding author.
E-mail address: roberto.brighenti@unifi.it (R. Brighenti).

https://doi.org/10.1016/j.euromechsol.2024.105323
Received 27 November 2023; Received in revised form 26 February 2024; Accepted 10 April 2024
Available online 14 April 2024

Nomenclature

A	Attenuation coefficient or material absorbance
$\mathscr{A}$	Depletion matrix of the light diffusion problem in the FE discretized domain
A_{abs}, A_{pol}, A_{mon}	Absorption due to photoabsorbers, due to monomer converted into polymer and due to un-polymerized monomers, respectively
b	Length of Kuhn's segments
c_a	Concentration of polymer's cross-link
C_I	Concentration of photo-initiator molecules (Ph_I)
C_M	Concentration of monomer molecules (M)
C_R	Concentration of free radicals ($R^\bullet$)
$\boldsymbol{S}$	Stabilization matrix of the numerical solution of the light diffusion problem
$\mathscr{E}$	Light gradient matrix of the domain discretized with FEs
$\boldsymbol{F}$	Deformation gradient tensor
$g(\boldsymbol{X}_0, \boldsymbol{X}, t)$	Dimensionless light intensity distribution at time t
$G, \overline{G}$	Shear modulus of the photopolimerized polymer and that of the fully-cured material, respectively
h_i	Thickness of the $i-th$ photopolymerized layer
$\mathscr{I}(\boldsymbol{X}, t)$	Light intensity field at time t
I_m	Maximum laser light intensity on the irradiated surface
$J = \det \boldsymbol{F}$	Relative volume change of the material
k_B	Boltzmann's constant
k_d, k_p, k_t	Reaction rate constants of the photopolymerization reactions
k_{pr}	Photodecomposition rate
$\boldsymbol{l}$	Unit vector identifying the incoming light beam direction
$\boldsymbol{L}$	Velocity tensor gradient of deformation
N	Number of Kuhn's segments in a polymer chain
$\boldsymbol{n}$	Unit vector normal to the free surface of the domain hit by the light beam
m	Number of radicals generated in the photodecomposition
$\boldsymbol{P}$	First Piola stress tensor
$P^\bullet$	Functional groups (growing polymer chains)
P_{dead}	Dead polymer chains (chains that completed the growth process)
$\boldsymbol{q}$	Vector of the nodal values of the incoming light intensity
$R^\bullet$	Free radicals
t	Time
t_c	Curing time
T	Temperature
v	Linear velocity of the light beam
$f(\boldsymbol{r}), f_0(\boldsymbol{r})$	Dimensionless distribution function of the chains' end-to-end vector and the corresponding one at the initial stress-free state, respectively
ψ	Energy in a single polymer chain
Ψ	Energy per unit volume of polymer
ϱ	Degree of cure (or degree of conversion, DoC) achieved during the photopolymerization
θ	Photo-initiator molar absorptivity
$[\blacksquare]$	Concentration of the chemical species represented by $\blacksquare$
$\widetilde{\blacksquare}$	Average value of the generic quantity $\blacksquare$

optimal control of material properties obtainable from the photopolymerization process has been the subject of the research proposed in (Classens et al., 2021); the Authors proposed a novel modular control-oriented paradigm for controlling the process, where the material properties are controlled in closed-loop and in real-time at the full machine scale. An interesting insight on the coupling between different physical phenomena involved in the production of ceramics through the AM photopolymerization process have been shown in (Westbeek et al., 2020); a theoretical and numerical framework – highlighting the difficulty in achieving homogeneous polymerization for ceramic-filled resins – has been presented. The parameters affecting the photopolymerization efficacy have been the subject of different investigations (Kılıç et al., 2021; Terrones et al., 2001; Lin et al., 2019; Bennett, 2017); based on experimental studies, the effect of layer thickness on residual monomers release in polymerization of bulk-fill composites has been presented in (Kılıç et al., 2021). In other studies, the kinetic equations have been derived and solved numerically to quantify the importance of accounting for the light attenuation and the photoinitiator consumption effects in photopolymerization (Terrones et al., 2001), and to evaluate the role of oxygen inhibition, viscosity, and variable light intensity due to photosensitizer depletion in time (Lin et al., 2019). The roles of the critical energy value necessary to initiate the polymerization and the penetration depth of the curing light for five commercial resins, have been considered through a testing methodology in (Bennett, 2017); the obtained results showed a wide range of values useful for improving the printer performance. Recently, experimental results aimed at quantifying the evolution of the degree of cure as a function of temperature and light intensity, rheometry-related quantities (such as the shear storage modulus in the gel–sol transition and beyond the gelation point), as well as for characterizing the shrinkage phenomenon in photopolymers obtained by DLP have been provided (Sekmen et al., 2022, 2023; Rehbein et al., 2021).

More recently, the implementation of artificial intelligence in this research field has been reported in a review paper in which the open issues, and the computational artificial intelligence models in photopolymerization-based 3D printing have been illustrated (Sachdeva et al., 2022).

In the present study, we investigate the photopolymerization process by quantifying the main involved physical processes and their reciprocal interaction; in more detail, we propose a multi-physics model describing the photopolymerization induced by a moving laser light source creating a layered structure. The mechanical response of the obtained material is finally considered and is related to the adopted photopolymerization printing setups.

The paper is organized as follows: Sect. 2 illustrates the governing equations of the chemical-physics phenomena involved in photopolymerization starting from light diffusion (Sect. 2.1), chemical kinetics (Sect. 2.2), and polymer mechanics (Sect. 2.3). Sect. 3 is devoted to the computational implementation of the proposed multi-physics model for layered photopolymerization. Sect. 4 presents some numerical results obtained by considering different settings of the photopolymerization-based AM process; some relevant conclusions and observations are drawn based on the material's mechanical properties distribution and the mechanical response of the obtained AM elements. Finally, Sect. 5 provides some conclusions and research perspectives in the field.

2. Chemical-physics of photopolymerization

In this section, the chemical-physics phenomena involved in the photopolymerization process are considered and the related governing equations are illustrated and discussed. Starting from the light spread and diffusion in the initially liquid medium being solidified, we consider the photo-induced chemical reactions leading to the solid polymer and, finally, we introduce a statistical-based description of the mechanics of the chain network to be used for the macroscale modelling of the material.

2.1. Light diffusion through a partially transparent medium

Light diffuses instantaneously in a partially or completely transparent material. The main parameter to be determined for this problem is the light intensity which attenuates as the light spreads deeper and deeper within the medium. The light intensity attenuation depends on the so-called absorptivity of the material, whose value depends on the amount of the various light-absorbing species present in the main material and on its own molar absorptivity.

The light diffusion is governed by the well-known Beer-Lambert law expressed by first order elliptic partial differential equations (PDEs) providing a relation between the light intensity gradient and the light attenuation (Davis and Marshak, 2004; Zakeri et al., 2020; Lang et al., 2022). Mathematically such a relationship is expressed as:

$$\begin{aligned} &\boldsymbol{l}(\boldsymbol{X},t)\cdot\nabla_{\boldsymbol{X}}\mathscr{I}(\boldsymbol{X},t) = -A(\boldsymbol{X},t)\,\mathscr{I}(\boldsymbol{X},t), \quad \boldsymbol{X}\in\Omega_0 \\ &\mathscr{I}(\boldsymbol{X},t) = \overline{\mathscr{I}}(\boldsymbol{X},t), \quad \boldsymbol{X}\in\partial\Omega_0 \end{aligned} \tag{1}$$

where Ω_0 is the domain through which the light spreads and $\partial\Omega_0$ is its boundary, while $\boldsymbol{X},t$ indicate the generic point belonging to the above-mentioned domain and the time, respectively. In Eq. (1), ∇_X indicates the gradient operator in the reference configuration, $\boldsymbol{l}(\boldsymbol{X},t)$ is the unit vector of the incoming beam light, $\mathscr{I}(\boldsymbol{X},t)$ is the light intensity at the time t at the point $\boldsymbol{X}$, and $A(\boldsymbol{X},t)$ is the light attenuation coefficient of the material. This latter parameter is usually expressed by adding the absorbances of the various species present in the material, namely - in the case of a photoresin - the photo-initiator (with concentration C_I) molar absorbivity θ, the photoabsorbers and polymer absorbivities A_{abs}, A_{pol}, respectively, and the absorbivity of the initial monomers A_{mon} (Shao et al., 2014), (Wu et al., 2018):

$$A(\boldsymbol{X},t) = \theta\, C_I(\boldsymbol{X},t) + A_{abs}(\boldsymbol{X},t) + A_{pol}\,\varrho(\boldsymbol{X},t) + A_{mon}[1-\varrho(\boldsymbol{X},t)] \tag{2}$$

The above expression considers the light absorbance to be evaluated by additively considering all the factors hindering the light beam in entering the material. As can be appreciated, $A(\boldsymbol{X},t)$ takes into account for the evolution of the various species involved in the process, namely the polymer-related light absorption effect through its fraction expressed by using the degree of cure ϱ, and the monomer-related light absorption effect through its residual amount, expressed by using the factor $1-\varrho$, taking place during the photopolymerization. The effects of the remaining quantities are assumed to be constant since the photo-initiator molecules and the photoabsorbers are permanently present in the material being solidified.

The above-stated problem has been equipped with Dirichlet boundary conditions providing the light intensity distribution over the irradiated boundary domain, $\mathscr{I}(\boldsymbol{X},t) = \overline{\mathscr{I}}(\boldsymbol{X},t)$, $\boldsymbol{X}\in\partial\Omega_0$, being the known light intensity distribution expressed as $\overline{\mathscr{I}}(\boldsymbol{X},t) = I_m\, g(\boldsymbol{X}_0,\boldsymbol{X},t)$, with g a dimensionless function (typically assumed to be a Gaussian distribution centered at $\boldsymbol{X}_0$) and $\mathscr{I}_m$ the maximum value of the light intensity here assumed to be constant.

It is worth noticing that in Eq. (2) the degree of cure $\rho(\boldsymbol{X},t)$ quantifying the fraction of liquid-solid conversion at the point $\boldsymbol{X}$ and time t has been introduced; since $A(\boldsymbol{X},t)$ depends on ϱ, the above PDEs expressed by (1) result to be non-linear.

2.2. Kinetics of the light-induced polymerization chemical reactions

Photopolymerization starts from a liquid material made of monomer units (M) with molecular concentration expressed by the function $C_M(\boldsymbol{X},t)$. Photo-initiators molecules (Ph_I), with concentration $C_I(\boldsymbol{X},t)$, are embedded in the liquid monomer and, upon light irradiation, are converted into m free radicals ($R^\bullet$) whose concentration is given by $C_R(\boldsymbol{X},t)$. Free radicals react with the monomer molecules promoting the activation of functional groups ($P^\bullet$) which, by reacting with monomer molecules, grow within the material leading to the formation of polymer chains (Fig. 1).

Growth and propagation of polymer chains proceed until a termination stage is achieved; this happens if a chain meets a free radical ($P^\bullet + R^\bullet \xrightarrow{k_t} P_{\text{dead}}$) or if a chain joins another chain encountered on its growing path ($P^\bullet + P^\bullet \xrightarrow{k_t} P_{dead}$) (Anastasio et al., 2019). The kinetic description of the reactions taking place during the polymerization can be summarized as follows:

$$\begin{aligned} &\textit{Photo}-\textit{initiators decomposition into 2 free radicals} \quad 1.\ Ph_I \xrightarrow{k_{pr}} mR^\bullet \\ &\textit{Onset of a polymer chain} \quad 2.\ R^\bullet + M \xrightarrow{k_p} P^\bullet \\ &\textit{Growth of a polymer chain} \quad 3.\ P^\bullet + M \xrightarrow{k_p} P^\bullet \\ &\textit{Termination of chains growth} \quad \begin{cases} 4a.\ P^\bullet + P^\bullet \xrightarrow{k_t} P_{dead} \\ 4b.\ P^\bullet + R^\bullet \xrightarrow{k_t} P_{dead} \end{cases} \end{aligned} \tag{3}$$

where k_{pr}, k_p and k_t are the kinetic rate constants (decomposition, propagation, and termination rates, respectively) characterizing the chemical process (Andrzejewska, 2001).

The above-described reactions are governed by the following kinetic models expressed by a set of first order PDEs providing the time rates of the photoinitiator, free radicals, and monomer units concentrations, respectively.

$$\dot{C}_I(\boldsymbol{X},t) = -\,k_{pr}\,\mathscr{I}(\boldsymbol{X},t)\,C_I(\boldsymbol{X},t) \tag{4a}$$

$$\dot{C}_R(\boldsymbol{X},t) = -\,m\,\dot{C}_I(\boldsymbol{X},t) - m\,k_t(\boldsymbol{X},t)[C_R(\boldsymbol{X},t)]^2 \tag{4b}$$

$$\dot{C}_M(\boldsymbol{X},t) = -\,k_p(\boldsymbol{X},t)C_M(\boldsymbol{X},t)C_R(\boldsymbol{X},t) \tag{4c}$$

with the initial conditions: $C_I(\boldsymbol{X},t=0) = C_{I0}, C_R(\boldsymbol{X},t=0) = C_{R0}$ and $C_M(\boldsymbol{X},t=0) = C_{M0}$, and $\dot{\blacksquare}$ indicates the time derivative operator applied to the quantity $\blacksquare$.

Other mechanisms, such as oxygen inhibition, should be also accounted for in the governing kinetic equations; in fact, the oxygen eventually present in the surrounding environment might reduce the polymerization reaction effectiveness by combining with radicals, thus slowing down the propagation of the polymer chains (Jariwala et al., 2011). It has also been experimentally demonstrated that the atmospheric oxygen inhibition and the molecular diffusion across layers are responsible for creating weak layers' interface (Gojzewski et al., 2020).

Neglecting the oxygen inhibition effect results in an overestimation of the degree of cure; however, in order not to involve too many parameters and side effects, in the present study we neglect such a phenomenon. Effective physical- (oxygen-free atmosphere) or chemical-based strategies can be introduced to reduce this detrimental effect (Ligon et al., 2014). The effect of photoinitiator concentration and of the laser intensity on the depth of curing in a polymerized gel has been studied in both experimentally and theoretically (Lee et al., 2001).

The photopolymerization process corresponds to a progressive reduction of the initial monomer concentration due to their consumption in forming the polymer chains whose concentration increases correspondingly. The degree of monomer-network chain formation is quantified through the Degree of Cure (DoC, degree of conversion), expressed as:

$$\varrho(\boldsymbol{X},t) = 1 - \frac{C_M(\boldsymbol{X},t)}{C_{M0}(\boldsymbol{X})} \tag{5}$$

being $C_{M0}(\boldsymbol{X}) = C_M(\boldsymbol{X}, t=0)$. When the material is made only of monomer units, i.e. at $t=0$, it is $\varrho(\boldsymbol{X},0) = 0$, and $\varrho(\boldsymbol{X},t)\to 1$ when all the monomer units disappear at a sufficiently high value of the curing time t. The field parameter $\varrho(\boldsymbol{X},t)$ is strictly related to the cross-link concentration $c_a(\boldsymbol{X},t)$ of the polymer, i.e. to the number of cross-link per unit

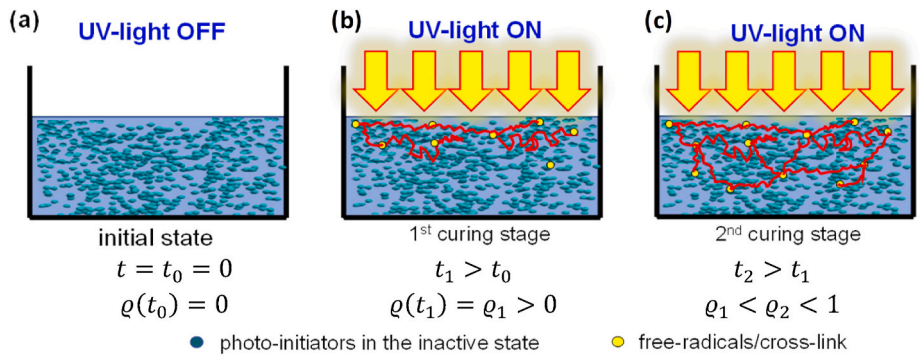

Fig. 1. Schematic of the photopolymerization process. Initially, the photo-initiators are inactive (a). When the resin is irradiated with the UV light, the photo-initiators are converted into free radicals (b) and react with the monomer molecules leading to the formation of the network of chains whose amount per unit volume is quantified by the so-called degree of cure $\varrho = \varrho(t)$ (c). (For interpretation of the references to colour in this figure legend, the reader is referred to the Web version of this article.)

volume; the degree of cure-cross-link concentration relationship can be expressed through the following equation (Zarrelli et al., 2010):

$$c_a(\boldsymbol{X},t) = \frac{1}{3\,k_B T}\left\{E_d + E_c\; e^{\left[u\left(\varrho(\boldsymbol{X},t)-\varrho_{gel}\right)\right]}\right\} \tag{6}$$

being k_B, T the Boltzmann's constant and the absolute temperature, respectively, while E_c, E_d and u are fitting parameters and ϱ_{gel} is the degree of cure at the so-called gelation point, i.e. when the material start becoming stiffer as the photopolymerization proceeds and is reflected in a loss in fluidity of the material. According to the rubber elasticity theory (Treloar, 1975), the cross-link density is related to the shear modulus G through the following relationship: $c_a(\boldsymbol{X},t) = G(\boldsymbol{X},t)/\,(k_B T)$.

From the above relations (4a) and (5) it appears that the evolution of the degree of cure at a given position of the material depends on the light intensity $\mathscr{I}(\boldsymbol{X},t)$ and its time history. The time rates of the degree of cure and of the cross-link concentration are given by:

$$\dot{\varrho}(\boldsymbol{X},t) = \frac{k_p(\boldsymbol{X},t)\; C_M(\boldsymbol{X},t)\; C_R(\boldsymbol{X},t)}{C_{M0}},\quad \dot{c}_a(\boldsymbol{X},t) = \frac{u\,E_c}{3\,k_B T}\; e^{\left[u\left(\varrho(\boldsymbol{X},t)-\varrho_{gel}\right)\right]}\;\dot{\varrho}(\boldsymbol{X},t) \tag{7}$$

and thus, the cross-link concentration at the curing time t_c can be easily evaluated by integrating $\dot{c}_a$ in the time domain:

$$c_a(\boldsymbol{X},t_c) = c_a(\boldsymbol{X},t=0) + \int_{t_{gel}}^{t_c} \dot{c}_a(\boldsymbol{X},t)\;dt \tag{8}$$

being $c_a(\boldsymbol{X},t=0) \cong c_{a,gel} \cong 0$ the initial value, reasonably assumed to be negligible, of the cross-link concentration of the material (practically at $t = t_{gel}$). It is worth recalling that for an infinite exposure time, the cross-link concentration tends to an asymptotic value corresponding to the so-called fully cured polymer whose shear modulus is $\overline{G} = G(c_a(t\to\infty))$.

2.3. Mechanics of a chain network

The typical constitutive models of polymer-like materials can either be represented by phenomenological (Treloar, 1943, 1944; Yeoh, 1990), or micromechanically-based approaches, the latter being based on linking the macroscopic mechanical response of the material to its molecular structure through statistical considerations (Arruda and Boyce, 1993; Diani and Le Tallec, 2019; Treloar and Riding, 1979). As a matter of fact, the mechanics of a polymeric material is conveniently provided by a statistical description of its chain network state; this approach results to be appropriate if the polymer's mechanical energy density is assumed to have an entropic nature. For a single chain, the mechanical energy is given by $\psi(|\boldsymbol{r}|) = -T\,s(|\boldsymbol{r}|)$ being $s(|\boldsymbol{r}|)$ the entropy, while $\boldsymbol{r}$ represents the chain's end-to-end vector. This approach is valid when the chains in the network are not too much stretched, i.e. if the applied stretch does not make the chains to approach their maximum possible extension, represented by the contour length bN, being b the length of a single Kuhn's segment (monomer unit forming the chain assumed to be not deformable) and N the number of segments in the chain (Doi, 2013). In the following, we adopt such a hypothesis to be valid, so the statistical description of the network will be used. A Gaussian distribution of the chain's end-to-end vector is usually adopted, i.e. $f_0(\lambda) = \left(\frac{3}{2\pi N b^2}\right)^{\frac{3}{2}} \exp\left(-\frac{3\lambda^2}{2}\right)$, where we have indicated with $\lambda = |\boldsymbol{r}|/|\boldsymbol{r}_0| = |\boldsymbol{r}|/(b\sqrt{N})$ the chain stretch, being $|\boldsymbol{r}_0| = b\sqrt{N}$ the mean end-to-end vector of the chain in the stress free state. The above distribution is characterized by mean value $\lambda = 1$ and standard deviation $\sqrt{1/3}$. Alternatively, the distribution function f in a generic state of the polymer can be also expressed in term of the chain's end-to-end vector, i.e. $f(\boldsymbol{r})$.

The mechanical energy density of the network in the stress-free state is obtained by adding up the energy values of all the chains embedded within such a volume:

$$\Psi_0 = c_a\langle f_0\,\psi\rangle = c_a\int_\Omega f_0\,\psi\;d\Omega \tag{9}$$

while the free energy density of the material is given by:

$$\Delta\Psi(t) = \Psi(t) - \Psi_0 = c_a\langle (f(t) - f_0)\,\psi\rangle \tag{10}$$

In the above relations, $\langle\blacksquare\rangle$ indicates the integration over the chain configuration space, i.e. over all the possible chains lengths and orientations ($\langle\blacksquare\rangle = \int_\Omega \blacksquare\, d\Omega = \int_0^{2\pi}\int_0^{\pi}\left(\int_0^{Nb}\blacksquare\, dr\right)\sin\theta\, d\theta\, d\omega$), and $f(t)$ is the distribution function at the time t. It is worth noticing that $\langle f_0\rangle = 1$ (Doi, 2013),(Vernerey et al., 2017).

Several possibilities for defining the energy ψ of a single chain exist: according to the Gaussian statistics $\psi(\lambda) = \frac{3k_B T\sqrt{N}}{2}\lambda^2$ (valid for low to moderate deformation states), while according to the Langevin statistics (valid also for large deformation states) $\psi(\lambda) = Nk_B T\cdot\left(\frac{\varphi}{bN}\lambda b\sqrt{N} + \ln\frac{\varphi}{\sinh\varphi}\right)$, with $\varphi = \mathscr{L}^{-1}\left(\frac{\lambda}{\sqrt{N}}\right)$, being $\mathscr{L}^{-1}$ the inverse of the Langevin function define as ($\mathscr{L}(\blacksquare) = \coth(\blacksquare) - \blacksquare^{-1}$) (Rubinstein et al., 2003).

The evolution of the chain distribution function can be easily obtained by evaluating its time rate:

$$\dot{f}(\boldsymbol{r}) = -\,\mathrm{div}\,[f(\boldsymbol{r})\,\dot{\boldsymbol{r}}] = -\,\nabla f\cdot\dot{\boldsymbol{r}} - f\nabla\cdot\dot{\boldsymbol{r}} = -\,(\nabla f\otimes\boldsymbol{r} + f\mathbf{1}) : \boldsymbol{L} \tag{11}$$

where $\dot{\boldsymbol{r}} = \boldsymbol{L}\boldsymbol{r} = \dot{\boldsymbol{F}}\boldsymbol{r}_0$ is the time rate of the end-to-end vector and $\boldsymbol{L} = \partial\,\dot{\boldsymbol{x}}/\partial\boldsymbol{X}$ is the velocity gradient whose 1st invariant is zero for any incompressible deformation, i.e. $\mathrm{tr}\,\boldsymbol{L} = L_{ii} = \mathbf{1} : \boldsymbol{L} = 0$ with $\mathbf{1}$ the second order unit tensor. It is worth mentioning that if volumetric shrinkage is

expected to occur in the photopolymerized material, it can be accounted for in Eq. (11) by determining the velocity gradient $\boldsymbol{L}$ corresponding to the constraint $[J - s_V(\varrho)] = 0$, being $s_V(\varrho) < 1$ the shrinkage volumetric function which in general depends on the degree of cure ϱ and temperature (Sekmen et al., 2023).

Finally, the stress state at a given point of the polymer is obtained as:

$$\boldsymbol{P}(t) = \frac{\partial \Delta \Psi(t)}{\partial \boldsymbol{F}} + p(t)\, J\, \boldsymbol{F}^{-T} \tag{12}$$

being $\boldsymbol{F}$ the deformation gradient tensor, $J = \det \boldsymbol{F} = 1$ for an incompressible deformation, while p is the corresponding hydrostatic constraint pressure. By considering Eq. (10), the 1st Piola stress tensor reads:

$$\boldsymbol{P}(t) = c_a \int_{\Omega} -(\nabla f \otimes \boldsymbol{r})\psi \, d\Omega : \boldsymbol{L}\, \dot{\boldsymbol{F}}^{-T} + p(t)\, J\, \boldsymbol{F}^{-T} \tag{13}$$

We assume that the mechanical deformation process takes place once the photopolymerization has been completed, so the cross-link concentration $c_a(\boldsymbol{X}, t_c) = c_\mu(\boldsymbol{X})$ used in Eqs (10) and (13) corresponds to the post-curing shear modulus of the material, $c_G(\boldsymbol{X}) = G(\boldsymbol{X})/(K_B T)$.

3. Computational framework

The above-described multi-physics model is suitable to be coded within a finite element (FE) framework. Firstly, the Beer-Lambert law is solved in the domain by assuming that the light hits the boundary of the domain whose position is made to vary according to the layer being printed. Starting from the bottom layer with thickness h_1, the moving light source (whose intensity is assumed to obey a Gaussian distribution, $I(X,t) = I_m \exp\frac{-(X-vt)^2}{c^2}$, where v is the linear (constant) velocity of the light beam, while c defines the width of the Gaussian distribution, Fig. 2a) is applied to the subsequent upper layers. While the light source is applied at the top edge of the $i-th$ layer, in the FE model the absorbance of the finite elements above such a layer is assumed to be very large in order to hinder the light spreading in the upward direction where the material (liquid nor solid) still does not exist (Fig. 2).

The multi-physics problem is solved numerically by adopting a finite element framework. Firstly, the light diffusion problem is considered for determining the light intensity field in the material domain being photopolymerized. The weak form of the light diffusion governing equations stated in (1) is introduced:

$$\begin{aligned} &\int_{\Omega_0} w(\boldsymbol{X})\, \boldsymbol{l}(\boldsymbol{X},t)\cdot\nabla_{\boldsymbol{X}} \mathscr{I}(\boldsymbol{X},t)\; dV = -\int_{\Omega_0} w(\boldsymbol{X})\, A(\boldsymbol{X},t)\, \mathscr{I}(\boldsymbol{X},t)\, dV \quad in \quad \Omega_0 \\ &\int_{\partial\Omega_0} w(\boldsymbol{X})\, \mathscr{I}(\boldsymbol{X},t)\, \bar{\boldsymbol{l}}(t)\cdot\boldsymbol{n}\, dS = I_m \int_{\partial\Omega_0} w(\boldsymbol{X})\, g(\boldsymbol{X},t)\, l_n\, dS \quad on \quad \partial\Omega_0 \end{aligned} \tag{14}$$

where w represents the test function and $[N]$, $[B]$ are suitable shape functions and compatibility matrix, respectively.

By introducing the nodal interpolation of the involved scalar quantities $\mathscr{I}$ and w and of their gradient within a single finite element having n_n nodes:

$$\begin{aligned} &\mathscr{I}_h(t) = \sum_{i=1}^{n_n} N_i \mathscr{I}_i(t), \quad \nabla_X \mathscr{I}_h(t) = \sum_{i=1}^{n_n} [B]_i \mathscr{I}_i(t), \\ &w_h = \sum_{i=1}^{n_n} N_i w_i, \quad \nabla_X w = \sum_{i=1}^{n_n} [B]_i\, w_i \end{aligned} \tag{15}$$

(where $\blacksquare_h$ indicates the interpolated variable and $\blacksquare_i$ the corresponding nodal value counterpart), upon assembling the involved matrices and vectors, the problem is expressed through a system of nonlinear equations in the form:

$$[\mathscr{E}(t) + \mathscr{A}(t) + \boldsymbol{S}]\, \mathscr{I}(t) = \boldsymbol{q}(t) \tag{16}$$

with

$$\begin{aligned} \mathscr{E}(t) &= \mathbb{A}_{e=1}^{ne} \left[\int_{V_e} [B]^T\, \bar{\boldsymbol{l}}(t) [N]\, dV \right]_e, \\ \mathscr{A}(t) &= \mathbb{A}_{e=1}^{ne} \left[-\int_{V_e} [N]^T A(\boldsymbol{X},t) [N]\, dV \right]_e, \\ \boldsymbol{S} &= \mathbb{A}_{e=1}^{ne} \left[Q h_e \int_{V_e} [B]^T [B]\, dV \right]_e, \\ \boldsymbol{q}(t) &= \mathbb{A}_{e=1}^{ne} \left[\int_{S_e} [N]^T g(\boldsymbol{X},t)\, l_n\, dS \right]_e \end{aligned} \tag{17}$$

In (16), the matrices $\mathscr{E}$, $\mathscr{A}$, $\boldsymbol{S}$ represent the light gradient matrix, the depletion matrix and the stabilization matrix of the discretized problem, respectively, while $\boldsymbol{q}(t)$ is the vector of the nodal values of the incoming light intensity on the boundary of the domain, and $\mathscr{I}$ is the vector of the unknown nodal light intensities (Brighenti et al., 2021b). In (17), $\mathbb{A}$ represents the assembly operator providing the overall matrices starting from those of the ne finite elements (whose volume and surface have been indicated with V_e and S_e, respectively) in which the domain has been discretized; finally, $Q\,(>1)$ is a coefficient (here assumed to be $Q = 2$) and h_e a characteristic small geometric size related to the problem required to define the stabilization matrix $\boldsymbol{S}$. This is required to avoid boundary layer problems (large gradients or oscillations of the solution) arising close to the boundary due to the presence of only the convective

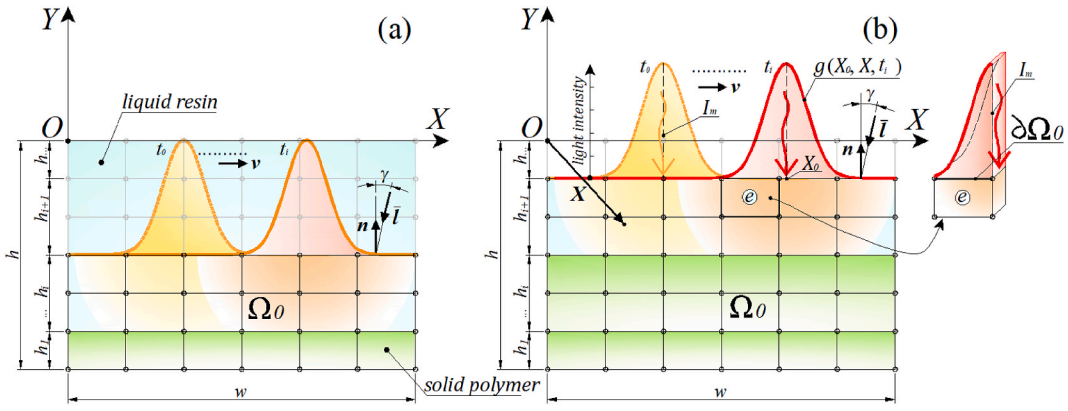

Fig. 2. Schematic of the photopolymerization process applied to layers of various thicknesses h_i. The light source moves from left to right at the velocity h to induce the photopolymerization starting from the bottom layer (a, b). The domain being printed is discretized with finite elements. The FE shape and size shown in this figure are not related to the FE meshes adopted in the numerical simulations presented in the following sections. (For interpretation of the references to colour in this figure legend, the reader is referred to the Web version of this article.)

(or transport) term $\boldsymbol{l}\cdot\nabla_X\mathscr{I}$ in the governing Eq. (1) (Quarteroni, 2014).

The light intensity distribution is obtained by solving in the time domain Eq (16); the essential boundary conditions are related to the upper surface of the domain directly hit by the light beam, while no significant light reflection is assumed to occur at the lateral boundaries nor at the underneath printed layers. In fact, the light beam crosses the material by progressively exponentially loosing intensity due to the absorbance effect.

Starting from the current light intensity field $\mathscr{I}(\boldsymbol{X},t)$ known at the FE nodal positions, the photopolymerization problem is solved by integrating in time Eqs (4a–4c), and Eqs (7) and (8) to determine the degree of cure and the cross-link density of the polymer at the FE Gauss points to be used to determine the shear material's modulus distribution at time t. It is worth mentioning that the evolution of the photoinitiator, free radicals, and monomer concentrations are determined by integrating Eq (4a) using the light intensity obtained in the 2D domain, i.e. by assuming that such a quantity does not change with the $z-$ coordinate (depth). From this perspective, the species concentration, i.e. expressed per unit volume of material to be used in the kinetics of photopolymerization (see Sect. 2.2), are consistent with the performed calculations.

After updating the concentrations of the involved species, the absorbance of the material expressed by Eq. (2) can be also updated and used in the subsequent time step for solving the light diffusion problem in a staggered way. For sake of simplicity, the absorbance of the material can be also considered to be constant through all the solution process; this assumption will be also considered in the numerical simulations in Sect. 4 and compared with cases where the absorbance is updated in time and space.

Finally, after completing the photopolymerization process for all the layers in which the domain has been subdivided, the mechanical properties of the material are known and the mechanical non-linear problem is solved with a standard numerical incremental procedure by considering the geometrical and mechanical nonlinearities, the latter coming from the micromechanical statistical-based model presented in Sect. 2.3 applied at the Gauss points level (Brighenti et al., 2021c). The above-described computational framework has been implemented in an in-house FE code operating in a staggered way: firstly, at a given time instant the light intensity distribution is determined and – by using such a distribution – the degree of cure field is determined in the domain together with the mechanical-related quantities. After completing the photopolymerization, the obtained mechanical characteristics of the material are adopted for solving the purely mechanical problem (where both mechanical (Sect. 2.3), and large displacement effects modelled in an updated Lagrangian framework, are accounted for), which is assumed to start after having completed the material solidification process.

4. Numerical examples

In the present section, some numerical examples based on the above-presented multi-physics model are illustrated. A simple rectangular domain with size $w = 30\ mm \times h = 10\ mm$ with depth 5 mm, discretized with 24×12 4-node elements, is considered. The photopolymerization process is assumed to take place in subsequent horizontal layers covering the entire domain starting from the bottom side of the domain being printed. The main parameters adopted for the kinetics of the chemical reactions are as follows: initial photo-initiator concentration $C_I(\boldsymbol{X}, t=0) = 20\ mol/m^3$, initial monomer concentration $C_M(\boldsymbol{X}, t=0) = 3000\ mol/m^3$, initial free radical concentration $C_R(\boldsymbol{X}, t=0) = 0\ mol/m^3$, photo-initiator decomposition rate $k_{pr} = 8 \bullet 10^{-4} m^2/J$, chain propagation and termination rates $k_p = k_t = 0.21\ m^3/mol{\cdot}s$, shear modulus of the fully cured material $\overline{G} = 267\ MPa$. The material is assumed to be in a plane stress condition.

In order not to include too many parameters in the numerical simulations which can make more difficult the interpretation of the results, in the following examples the simplest case of a constant light absorbance, unless differently stated, is assumed to be $A(\boldsymbol{X},t) = 600\ m^{-1}$. It is worth noticing that with such an absorbance, in a simple one dimensional setting the light intensity, $I(z,t) = I_0(t)\exp(-Az)$, attenuates from I_0 to 0.1 I_0 at a depth of about $z = 3.8{\cdot}10^{-3}\ m$, corresponding nearly to five FE size. The cases presented in Sect. 4.2 considering a variable light absorbance of the material have been simulated by updating $A(\boldsymbol{X},t)$ at the FE Gauss points through the use of Eq. (2) where the absorbance is function of the evolving quantities $C_I(\boldsymbol{X},t)$, $A_{abs}(\boldsymbol{X},t)$, $\varrho(\boldsymbol{X},t)$. After completing the photopolymerization process performed according to the printing setup assumed in the various cases, its overall mechanical response is numerically simulated by adopting the mechanical model illustrated in Sect. 2.3.

4.1. Polymer printing by keeping constant the total photopolymerization energy

In this first set of examples, we consider the printing procedure applied to the above-mentioned domain by keeping constant the total energy used; this condition corresponds to a constant product of the light intensity and the total curing time which have been assumed to be constant in all the examined cases, equal to $I_m = 100\ W/m^2$ (with $c = 10^{-3}\ m$), $t_c = 15\ s$, photopolymerization time step $dt = 0.1\ s$, respectively. Three cases characterized by: one layer ($h_l = h = 10\ mm, v = 2\ mm/s$), two layers ($h_l = h/2 = 5\ mm, v = 4\ mm/s$), and three layers ($h_l = h/3 = 3.33\ mm, v = 6\ mm/s$) covering the entire printing domain are considered, while a constant value of the absorbance is assumed in all cases.

In Fig. 3 the maps of the degree of cure obtained at the end of the process for the three considered cases are represented, while Fig. 4a–c illustrates the corresponding dimensionless shear modulus distribution. It is worth noticing that the variation of the depth of the cured material taking place during the photopolymerization process, depends on the light moving direction (from left to right) on top of the domain. A detailed description of the solidification process taking place in the initially liquid monomer domain is outlined in Sect. 4.2 where the evolution of the involved chemical species is illustrated in Figs. 8 and 9.

Finally, Fig. 4d shows how the mechanical response of the printed cantilever beam results to be much stiffer if printed in one layer, being the photopolymerization process performed in a longer curing time devoted to such a single layer; obviously, the material appears to be less homogeneous in term of the shear modulus distribution. It is worth observing that the emerging nonlinear response of the element comes from both the nonlinear mechanical hyperelastic behaviour of the material illustrated in Sect. 2.3, and from the large displacement effect here considered in the FE calculations. Further, since the photopolymerization is performed by adopting a constant overall curing time, it is expected that the amount of solid material created is approximately the same in all cases even if differently distributed in the domain.

4.2. Printing by adopting a constant curing time per layer

In this case, we consider printing the material by adopting a different number of layers to be photopolymerized by irradiation with a light moving at a constant speed or, equivalently, by adopting a constant curing time per layer, $t_{c,l} = 10\ \mathrm{s}\ (v_l = 3\ \mathrm{mm/s})$. The maximum light intensity is assumed to be constant, $I_m = 100\ W/m^2$. In this case the energy required to solidify the domain is different in the various cases. Four cases are considered, namely one layer, $h_l = h = 10\ mm, t_c = 10\ s$, two layers, $h_l = h/2 = 5\ mm,\ t_c = 20\ s$, three layers, $h_l = h/3 = 3.33\ mm, t_c = 30\ s$, and four layers, $h_l = h/4 = 2.5\ mm, t_c = 40\ s$. The overall curing time results to be $t_c = N\ t_{c,l}$, being N_l the number of layers. Each numerical simulation related to the 40 s long printing process, requires about 320 s calculation time on a desktop computer

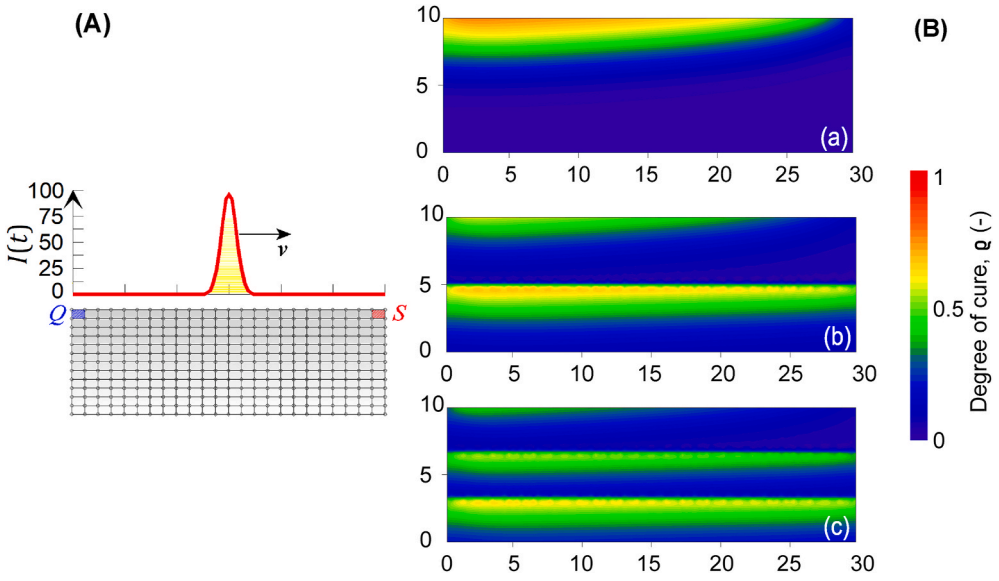

Fig. 3. FE discretized domain and assumed distribution of the light intensity; the light moves from left to right on the top edge of the domain (A). Maps of the degree of cure at the end of the photopolymerization process ($t/t_c = 1$), by adopting $I_m = 100\ W/m^2$ and $t_c = 15\ s$. The three printing setups are characterized by a constant value of the energy supplied to the material, i.e. $t_c \cdot I_m = const$. The domain is printed by adopting one (a), two (b) and three (c) layers whose thickness is $h_l = h;\ h/2;\ h/3$, respectively. Correspondingly, the laser speed is $v_l = v = \frac{2mm}{s}; v_l = 2v; v_l = 3v$ (a,b,c) (B). Geometrical dimensions in mm.

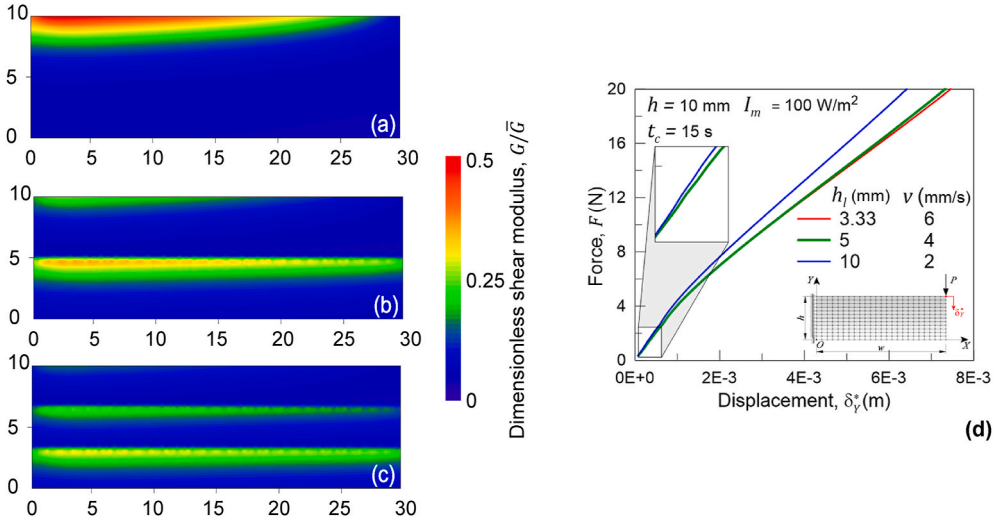

Fig. 4. *Maps of the dimensionless shear modulus $G/\overline{G}$ at the end of the photopolymerization process ($t/t_c = 1$), by adopting $I_m = 100\ W/m^2$ and $t_c = 15\ s$. The three printing setups are characterized by a constant value of the energy supplied to the material. The domain is printed by adopting one (a), two (b) and three (c) layers whose thickness is $h_l = h;\ h/2;\ h/3$, respectively. Correspondingly, the laser speed is $v_l = v;\ 2v;\ 3v$ (a,b,c). Load-displacement curves of the photopolymerized element loaded with a transversal force F (d); response corresponding to the three different printing setups shown in a,b,c. Geometrical dimensions in mm.*

equipped with an i-7-7700 CPU and 64 Gb RAM.

Firstly, the degree of cure obtained after printing only the first layer when the absorbance is assumed to be constant is illustrated in Fig. 5, while Fig. 6 shows the maps of the degree of cure at the end of the printing process for the 4 considered cases when both constant and variable light absorbance is assumed.

The value of the absorbance during the photopolymerization process is evaluated by using Eq. (2) by adopting the following parameters: initial photo-initiators concentration $C_I(\boldsymbol{x},0) = 20\ mol/m^3$; initial liquid monomer concentration $C_M(\boldsymbol{x}, t=0) = 3000\ mol/m^3$; photo-initiators molar absorptivity $\theta = 30\ m^2/\ mol$. Moreover, the absorbance adopted for a fully cured polymer and for the initial liquid monomer material are respectively, $A_{pol} = 2400\ m^{-1}$ and $A_{mon}(\boldsymbol{X}, t) = 0$ (infinitely transparent), while no photoabsorbers are considered to exist the initial material ($A_{abs}(\boldsymbol{X}, t) = 0$). These parameters allow the absorbance to range from $A = 600\ m^{-1}$ when curing doesn't exists yet ($\varrho(\boldsymbol{X}, 0) = 0$, corresponding to the purely liquid material), to the value of a fully cured condition ($\varrho(\boldsymbol{X}, t \to \infty) = 1$, fully solid polymer) corresponding to $A = 2400\ m^{-1}$ (Wu et al., 2018), (Bartolo, 2007).

By comparing Fig. 5, Fig. 6, Fig. 7, and Fig. 8 it can be appreciated that printing the same domain in multiple smaller layers enable the polymer to be more effectively cured, corresponding to a better polymerized material.

It is worth noticing that the more realistic case of a variable absorbance leads to different results in term of DOC (Fig. 6a1-d1) and of the dimensionless shear modulus (Fig. 8a1-d1) whose variation across a vertical cross-section of the printed material is shown in Fig. 11. The loss of transparency of the material due to the solidification process, hinders

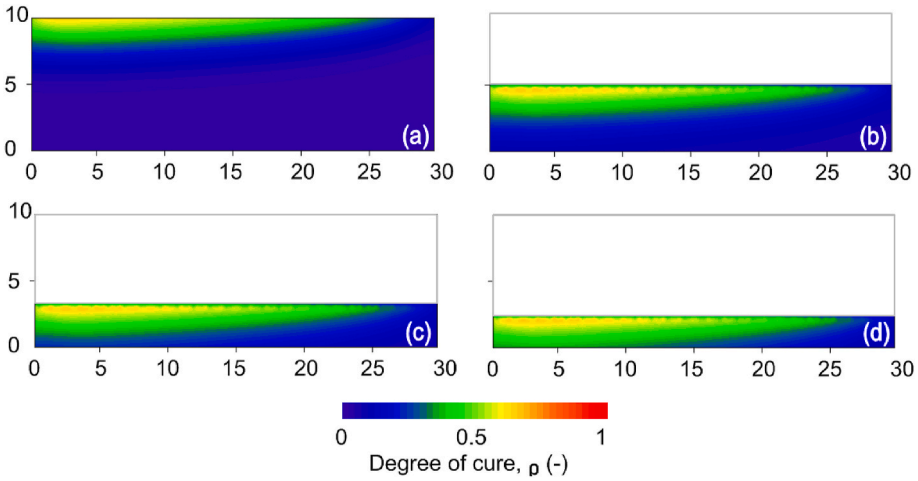

Fig. 5. Maps of the degree of cure at $t = 10\,s$, i.e. when only the first layer has been photopolymerized, for various printing setups with one (a), two (b), three (c), and four (d) layers having thickness $h_l = h;\ \ h/2;\ \ h/3;\ \ h/4$, respectively. The light absorbance A is assumed to be constant. The corresponding curing times for the whole domain are $t_c = t_{c,l};\ \ t_c = 2t_{c,l};\ \ t_c = 3t_{c,l};\ \ t_c = 4t_{c,l}$. The light source has maximum intensity equal to $I_m = 100\ W/m^2$ and moves on each layer at a constant speed $v_l = 3\ mm/s$. Geometrical dimensions in mm.

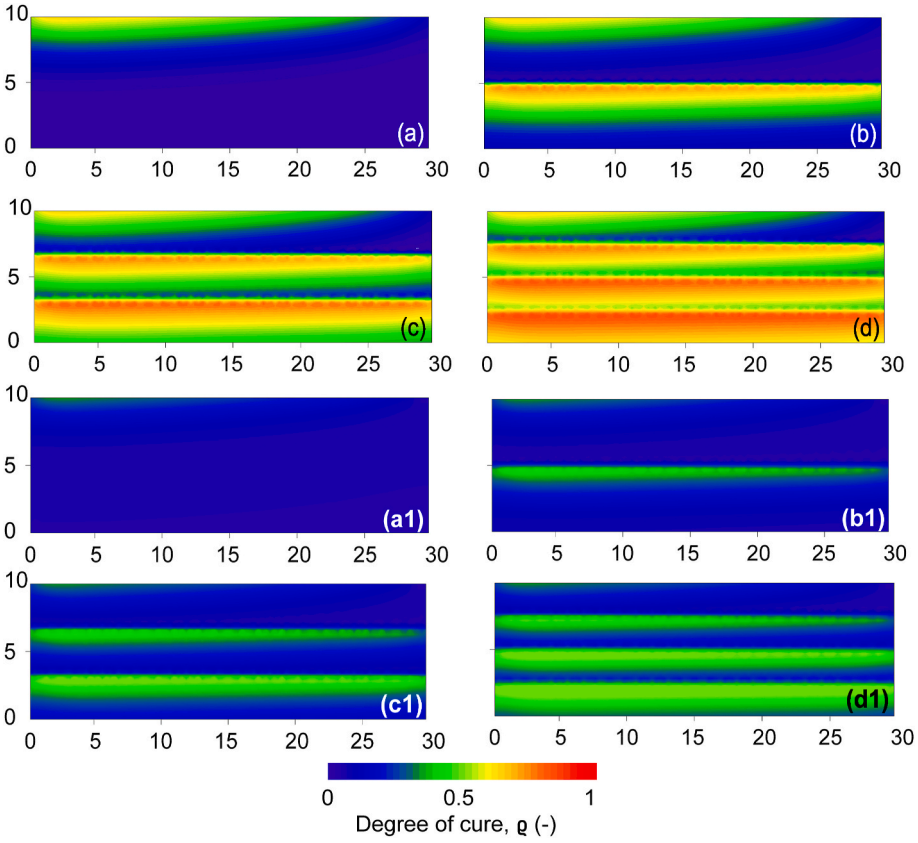

Fig. 6. Maps of the degree of cure at the end of the photopolymerization process for various printing setups with one (a), two (b), three (c), and four (d) layers having thickness $h_l = h;\ \ h/2\ \ ;h/3;\ \ h/4$, respectively. Cases (a–d) refer to a constant absorbance, cases (a1-d1) refer to a variable absorbance (see Eq. (2)). The corresponding curing times for the whole domain are $t_c = t_{c,l};\ \ t_c = 2t_{c,l};\ \ t_c = 3t_{c,l};\ \ t_c = 4t_{c,l}$. The light source has maximum intensity $I_m = 100\ W/m^2$ and moves on each layer at a constant speed $v_l = 3\ mm/s$. Geometrical dimensions in mm.

an effective light spread in the domain with the consequence of reducing the degree of polymerization. However, irrespectively of the absorbance value within the domain being solidified, printing in multiple thinner layers is more effective that printing subsequent layers with a larger thickness.

Finally, the mechanical response of the polymer photopolymerized by adopting different numbers of layers is shown in Fig. 7e when a constant absorbance is adopted. It appears that, thanks to the higher cross-link density obtained at the end of the printing process, the case with four layers results to be the stiffest one (see Fig. 8d).

In order to explain the thickness variation of the degree of cure of regions of material placed along the horizontal direction, we consider

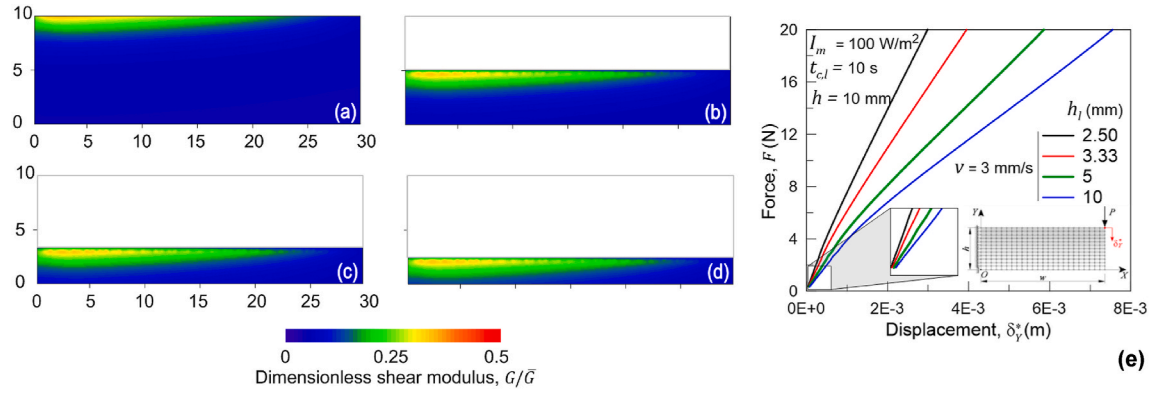

Fig. 7. Maps of the dimensionless shear modulus at $t = 10\ s$ (i.e. when only the first layer has been photopolymerized), for various printing setups with one (a), two (b), three (c), and four (d) layers having thickness $h_l = h;\ \ h/2;\ \ h/3;\ \ h/4$, respectively. The light absorbance A is assumed to be constant. The corresponding curing times for the whole domain are $t_c = t_{c,l};\ t_c = 2t_{c,l};\ t_c = 3t_{c,l};\ t_c = 4t_{c,l}$. The maximum intensity of the light source is $I_m = 100\ W/m^2$ and moves on each layer at a constant speed $v_l = 3\ mm/s$. Geometrical dimensions in mm. Load-displacement curves corresponding to the four different considered printing setups of the photopolymerized element loaded with a transversal force (e).

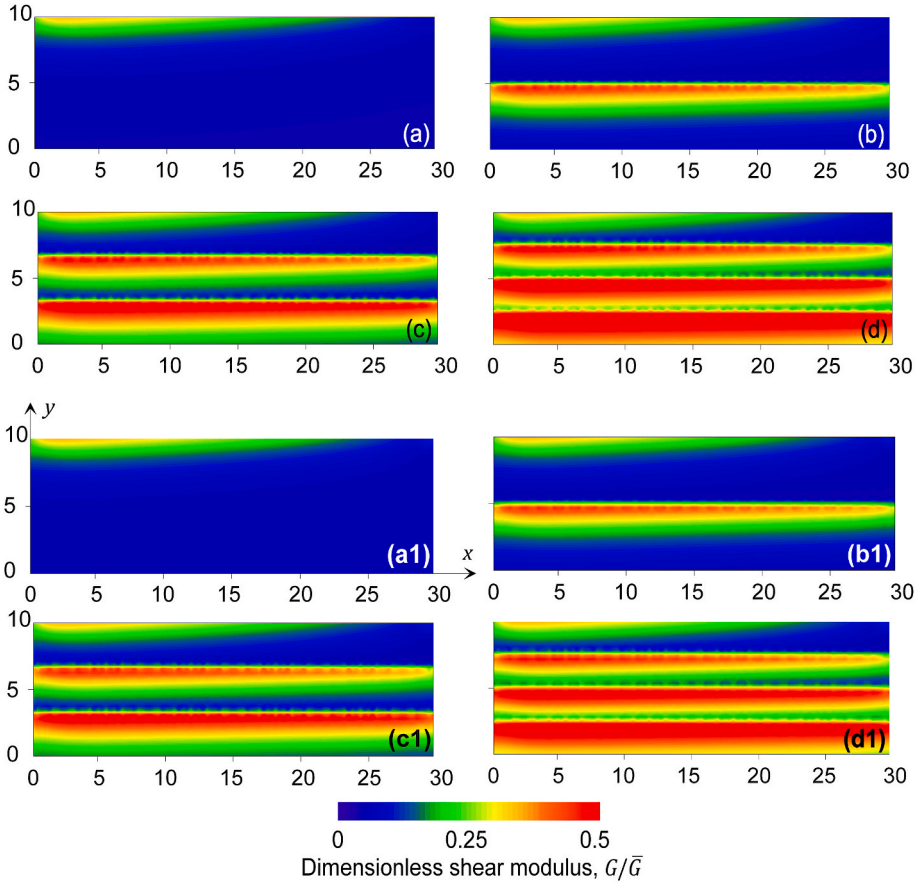

Fig. 8. Maps of the dimensionless shear modulus at the end of the photopolymerization process for various printing setups with one (a), two (b), three (c), and four (d) layers having thickness $h_l = h;\ \ h/2;\ \ h/3;\ \ h/4$, respectively. Cases (a–d) refer to cases with constant absorbance A, cases (a1-d1) refer to cases with variable absorbance. The corresponding curing times for the whole domain are $t_c = t_{c,l};\ t_c = 2t_{c,l};\ t_c = 3t_{c,l};\ t_c = 4t_{c,l}$. The light source has a maximum intensity $I_m = 100\ W/m^2$ and moves on each layer at a constant speed $v_l = 3\ mm/s$. Geometrical dimensions in mm.

here a deeper study of the chemical species evolution at two representative points (Q and S, see Fig. 3A) placed at extremities of the top surface of the domain. In particular, we consider case (d) of Fig. 8 which is characterized by four printed layers with identical thickness, curing light moving from left to right, and constant absorbance. In Fig. 9 the variation in time of the light intensity (Fig. 9a), of the photo-initiator concentration (Fig. 9b), of the free radical concentration (Fig. 9c), and of the monomer concentration (Fig. 9d) *vs* time are shown. When the initially liquid material is irradiated by light, the photoinitiator decomposition starts with the formation of free radicals which keep consuming the monomer molecules leading to the formation of the polymer chain. This process continues also when the light has moved away and the point is not any more directly irradiated, thus justifying a more pronounced polymer chain formation.

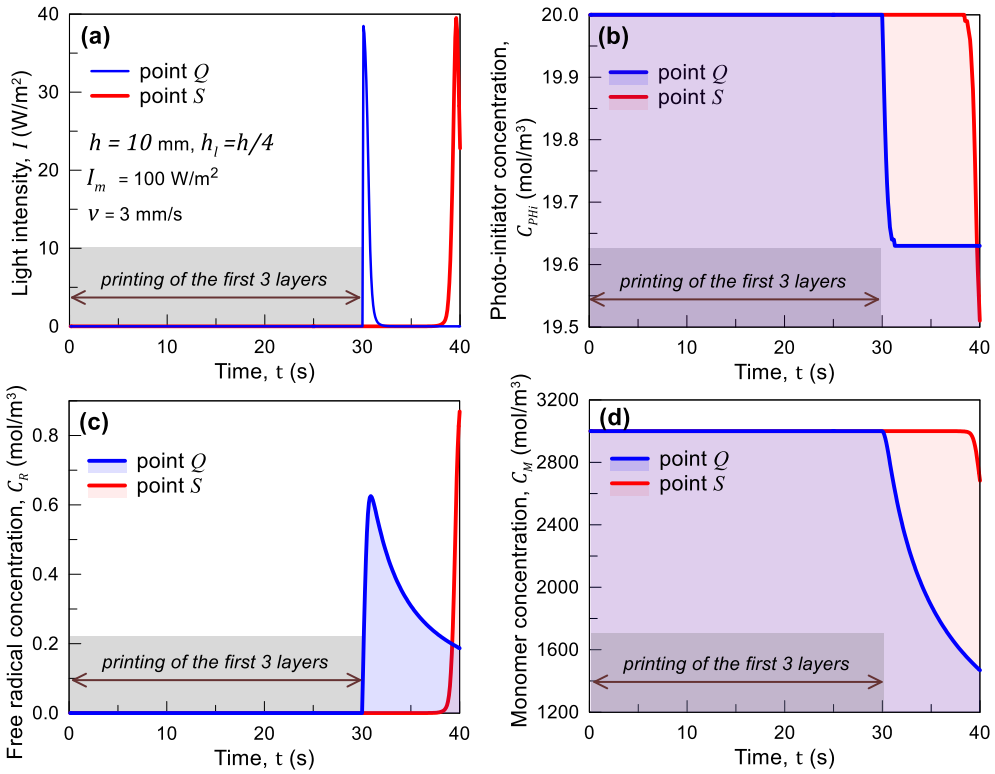

Fig. 9. Evolution of the degree of cure at points Q and S (see Fig. 3A), belonging to the top surface of the domain being printed (4th layer), for the case illustrated in 8d.

From Fig. 9a it can be easily appreciated that the total amount of free radicals formed during the process (proportional to the area under the $C_R(t)$ curve) is higher at point Q with respect to point S, and also the monomer units present in the unit volume C_M is lower at point Q, meaning that more polymer chains are formed at that location. Correspondingly, the degree of cure at point Q results to be higher than at point S (Fig. 10), thus justifying the better curing degree of the material placed in the left-hand side region of the domain.

Across two subsequent printed layers, a huge variation of the shear modulus takes place. In (Gojzewski et al., 2020), a detailed micro scale experimental study has been conducted to quantify the layers' interface weakness; the Young's modulus across the layered structure has been determined by atomic force microscopy (AFM).

In Fig. 12 the dimensionless shear modulus measured across two subsequent printed layers (Gojzewski et al., 2020) and that obtained from the present model are shown. It can be appreciated that the trend shown by the shear modulus vs the distance from the layers' interface is well captured by the present model.

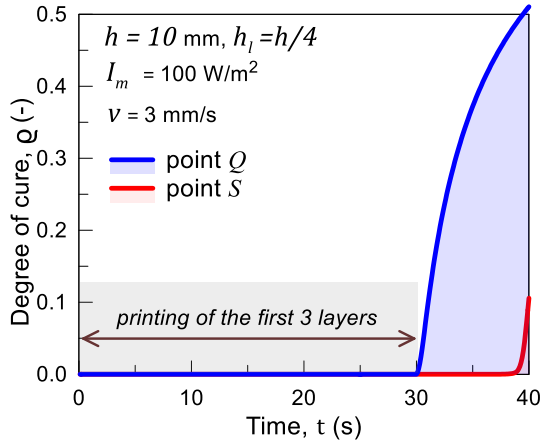

Fig. 10. Evolution of the degree of cure at points Q and S, belonging to the top surface of the domain being printed (4th layer), for the case illustrated in 8d.

5. Conclusions and future perspectives

The photopolymerization process represents an efficient technology to obtain a solid polymer starting from a liquid resin made of monomer units, whose polymerization (chain formation and cross-linking) is obtained by exposing the raw material to a light source of proper wavelength. This technology enables obtaining objects with high dimensional precision and spanning a wide range of geometrical sizes and is widely used in additive manufacturing. The chemical-physics processes on which this process is based, allow tailoring the distribution of the material's characteristics: controlling how the light-induced polymerization process is performed, namely the light intensity, the light source speed, the layers' thickness, etc., enable to easily control the distribution of the polymer's physical and mechanical properties. In the present study, we have illustrated the main chemical-physics phenomena involved in photopolymerization and how they can be quantitatively described through the relevant governing equations.

In particular, we have considered the light diffusion within a partially transparent medium and how the light intensity and its duration at a given point of the material domain can be used to tune the degree of cure, corresponding to the obtainable degree of cross-link density of the polymer network at that position. Printing the domain of interest by adopting different layer arrangements and light source speeds, has demonstrated how different can be the distribution of the mechanical properties of the material within the cured domain. Also the evolution of the material's light absorbance, corresponding to the degree of transparency of the medium, plays a crucial role in determining the property distribution of the final printed part. Changing the light intensity during the photopolymerization process, despite being not usually available in commercial AM procedures, offers a further

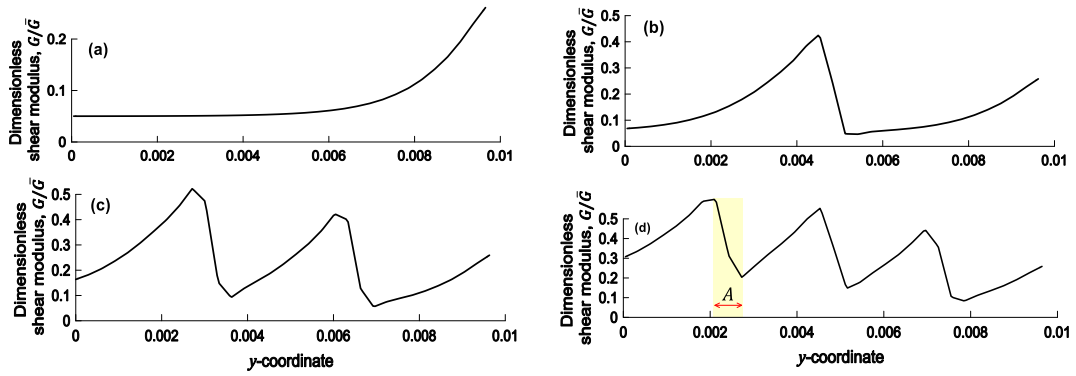

Fig. 11. Dimensionless shear modulus along a vertical cross-section placed at $x = 0.015\,m$. Cases a, b, c, and d of the present figure correspond to cases a1, b1, c1, and d1 in Fig. 8. Distances in the y-direction are expressed in m.

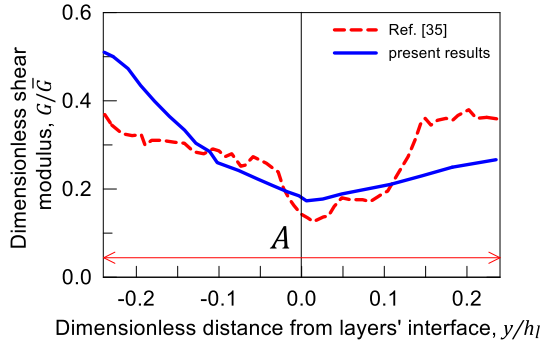

Fig. 12. Dimensionless shear modulus across two subsequently printed layers. Results from (Gojzewski et al., 2020) and from the present computational simulation (see Fig. 11d) are reported.

possibility of tuning the mechanical properties architecture within the domain.

Photopolymerization represents an advanced tool for creating solid objects with highly controllable distribution values of their physical characteristic; the use of machine learning-based approaches, for instance, can straightforwardly enable to determine the optimal printing setup to achieve the desired mechanical response under prescribed boundary conditions, leading to continuum engineered materials as an alternative to discontinuous metamaterials usually adopted for such a purpose.

CRediT authorship contribution statement

Roberto Brighenti: Writing – original draft, Supervision, Funding acquisition, Conceptualization. **Mattia P. Cosma:** Investigation. **Silvia Monchetti:** Writing – review & editing.

Declaration of competing interest

The authors declare that they have no known competing financial interests or personal relationships that could have appeared to influence the work reported in this paper.

Data availability

Data will be made available on request.

Acknowledgments

RB and MPC would like to thank the support from European Union's Horizon 2020 research and innovation programme (H2020-WIDESPREAD-2018, SIRAMM) under grant agreement No 857124.

References

Al Rashid, A., Ahmed, W., Khalid, M.Y., Koc, M., 2021. Vat photopolymerization of polymers and polymer composites: processes and applications. Addit. Manuf. 47, 102279 https://doi.org/10.1016/j.addma.2021.102279.

Anastasio, R., Peerbooms, W., Cardinaels, R., Van Breemen, L.C.A., 2019. Characterization of ultraviolet-cured methacrylate networks: from photopolymerization to ultimate mechanical properties. Macromolecules 52, 9220–9231. https://doi.org/10.1021/acs.macromol.9b01439.

Andrzejewska, E., 2001. Photopolymerization kinetics of multifunctional monomers. Prog. Polym. Sci. 26, 605–665. https://doi.org/10.1016/S0079-6700(01)00004-1.

Andrzejewska, E., Grajek, K., 2017. Recent advances in photo-induced free-radical polymerization. MOJ Polymer science 58–60. https://doi.org/10.15406/mojps.2017.01.00009.

Arruda, E.M., Boyce, M.C., 1993. A three-dimensional constitutive model for the large stretch behavior of rubber elastic materials. J. Mech. Phys. Solid. 41 (2), 389–412. https://doi.org/10.1016/0022-5096(93)90013-6.

Bartolo, P.J. da S., 2007. Photo-curing modelling: direct irradiation. Int. J. Adv. Manuf. Technol. 32 (5–6), 480–491. https://doi.org/10.1007/s00170-005-0374-5.

Bella, F., Bongiovanni, R., 2013. Photoinduced polymerization: an innovative, powerful and environmentally friendly technique for the preparation of polymer electrolytes for dye-sensitized solar cells. J. Photochem. Photobiol. C Photochem. Rev. 16, 1–21. https://doi.org/10.1016/j.jphotochemrev.2013.03.002.

Bennett, J., 2017. Measuring UV curing parameters of commercial photopolymers used in additive manufacturing. Addit. Manuf. 18, 203–212. https://doi.org/10.1016/j.addma.2017.10.009.

Bikas, H., Stavropoulos, P., Chryssolouris, G., 2016. Additive manufacturing methods and modelling approaches: a critical review. Int. J. Adv. Des. Manuf. Technol. 83, 389–405. https://doi.org/10.1007/s00170-015-7576-2.

Bowman, C.N., Kloxin, C.J., 2008. Toward an enhanced understanding and implementation of photopolymerization reactions. AIChE J. 54, 2775–2795. https://doi.org/10.1002/aic.11678.

Brighenti, R., Cosma, M.P., Marsavina, L., Spagnoli, A., Terzano, M., 2021a. Laser-based additively manufactured polymers: a review on processes and mechanical models. J. Mater. Sci. 56, 961–998. https://doi.org/10.1007/s10853-020-05254-6.

Brighenti, R., Cosma, M.P., Marsavina, L., Spagnoli, A., Terzano, M., 2021b. Multiphysics modelling of the mechanical properties in polymers obtained via photo-induced polymerization. Int. J. Adv. Des. Manuf. Technol. 117 (1–2), 481–499. https://doi.org/10.1007/s00170-021-07273-2.

Brighenti, R., Cosma, M.P., 2021c. Mechanical behavior of photopolymerized materials. J. Mech. Phys. Solid. 153, 104456 https://doi.org/10.1016/j.jmps.2021.104456.

Buss, B.L., Miyake, G.M., 2018. Photoinduced controlled radical polymerizations performed in flow: methods, products, and opportunities. Chem. Mater. 30, 3931–3942. https://doi.org/10.1021/acs.chemmater.8b01359.

Chen, M., Zhong, M., Johnson, J.A., 2016. Light-controlled radical polymerization: mechanisms, methods, and applications. Chem. Rev. 116, 10167–10211. https://doi.org/10.1021/acs.chemrev.5b00671.

Classens, K., Hafkamp, T., Westbeek, S., Remmers, J.J., Weiland, S., 2021. Multiphysical modeling and optimal control of material properties for photopolymerization processes. Addit. Manuf. 38, 101520 https://doi.org/10.1016/j.addma.2020.101520.

Davis, A.B., Marshak, A., 2004. Photon propagation in heterogeneous optical media with spatial correlations: enhanced mean-free-paths and wider-than-exponential free-path distributions. J. Quant. Spectrosc. Radiat. Transf. 84, 3–34. https://doi.org/10.1016/S0022-4073(03)00114-6.

Diani, J., Le Tallec, P., 2019. A fully equilibrated microsphere model with damage for rubberlike materials. J. Mech. Phys. Solid. 124, 702–713. https://doi.org/10.1016/j.jmps.2018.11.021.

Doi, M., 2013. Soft Matter Physics. Oxford University Press, USA.

Gojzewski, H., Guo, Z., Grzelachowska, W., Ridwan, M.G., Hempenius, M.A., Grijpma, D. W., Vancso, G.J., 2020. Layer-by-layer printing of photopolymers in 3D: how weak is

the interface? ACS Appl. Mater. Interfaces 12 (7), 8908–8914. https://doi.org/10.1021/acsami.9b22272.
Han, D., Yang, C., Fang, N.X., Lee, H., 2019. Rapid multi-material 3D printing with projection micro-stereolithography using dynamic fluidic control. Addit. Manuf. 27, 606–615. https://doi.org/10.1016/j.addma.2019.03.031.
Jariwala, A.S., Ding, F., Boddapati, A., Breedveld, V., Grover, M.A., Henderson, C.L., Rosen, D.W., 2011. Modeling effects of oxygen inhibition in mask-based stereolithography. Rapid Prototyp. J. 17 (3), 168–175. https://doi.org/10.1108/13552541111124734.
Kılıç, V., Hurmuzlu, F., Ugur, Y., Cangul, S., 2021. Effect of layer thickness on residual monomer release in polymerization of bulk-fill composites. Polym. Polym. Compos. 29 (9_Suppl. l), S296–S305. https://doi.org/10.1177/0967391121999588.
Lang, M., Hirner, S., Wiesbrock, F., Fuchs, P., 2022. A review on modeling cure kinetics and mechanisms of photopolymerization. Polymers 14 (10), 2074. https://doi.org/10.3390/polym14102074.
Lee, J.H., Prud'Homme, R.K., Aksay, I.A., 2001. Cure depth in photopolymerization: experiments and theory. J. Mater. Res. 16 (12), 3536–3544. https://doi.org/10.1557/JMR.2001.0485.
Ligon, S.C., Husár, B., Wutzel, H., Holman, R., Liska, R., 2014. Strategies to reduce oxygen inhibition in photoinduced polymerization. Chem. Rev. 114 (1), 557–589. https://doi.org/10.1021/cr3005197.
Lin, J.T., Liu, H.W., Chen, K.T., Cheng, D.C., 2019. Modeling the kinetics, curing depth, and efficacy of radical-mediated Photopolymerization: the role of oxygen inhibition, viscosity, and dynamic light intensity. Front. Chem. 7, 760. https://doi.org/10.3389/fchem.2019.00760.
Long, K.N., Scott, T.F., Qi, H.J., Bowman, C.N., Dunn, M.L., 2009. Photomechanics of light-activated polymers. J. Mech. Phys. Solid. 57 (7), 1103–1121. https://doi.org/10.1016/j.jmps.2009.03.003.
Phillips, R., 1984. Photopolymerization. J. Photochem. 25, 79–82. https://doi.org/10.1016/0047-2670(84)85016-9.
Quarteroni, A., 2014. Numerical Models for Differential Problems, second ed. Springer, Berlin, pp. 291–338. https://doi.org/10.1007/978-88-470-5522-3.
Rehbein, T., Johlitz, M., Lion, A., Sekmen, K., Constantinescu, A., 2021. Temperature- and degree of cure-dependent viscoelastic properties of photopolymer resins used in digital light processing. Progress in Additive Manufacturing 6 (4), 743–756. https://doi.org/10.1007/s40964-021-00194-2.
Rubinstein, M., Colby, R.H., 2003. Polymer Physics. Oxford University Press.
Sachdeva, I., Ramesh, S., Chadha, U., Punugoti, H., Selvaraj, S.K., 2022. Computational AI models in VAT photopolymerization: a review, current trends, open issues, and future opportunities. Neural Comput. Appl. 34 (20), 17207–17229. https://doi.org/10.1007/s00521-022-07694-4.
Schwartz, J.J., 2022. Additive manufacturing: frameworks for chemical understanding and advancement in vat photopolymerization. MRS Bull. 47 (6), 628–641. https://doi.org/10.1557/s43577-022-00343-0.
Sekmen, K., Rehbein, T., Johlitz, M., Lion, A., Constantinescu, A., 2022. Thermal analysis and shrinkage characterization of the photopolymers for DLP additive manufacturing processes. Continuum Mech. Therm. 1–18. https://doi.org/10.1007/s00161-022-01137-0.
Sekmen, K., Rehbein, T., Johlitz, M., Lion, A., Constantinescu, A., 2023. Curing-dependent thermo-viscoelastic and shrinkage behaviour of photopolymers. Mech. Mater. 179, 104566 https://doi.org/10.1016/j.mechmat.2023.104566.
Shao, J., Huang, Y., Fan, Q., 2014. Visible light initiating systems for photopolymerization: status, development and challenges. Polym. Chem. 5, 4195–4210. https://doi.org/10.1039/C4PY00072B.
Terrones, G., Pearlstein, A.J., 2001. Effects of optical attenuation and consumption of a photobleaching initiator on local initiation rates in photopolymerizations. Macromolecules 34 (10), 3195–3204. https://doi.org/10.1021/ma001235y.
Treloar, L.R.G., 1943. The elasticity of a network of long-chain molecules-ii. Trans. Faraday Soc. 39, 241–246. https://doi.org/10.1039/TF9433900241.
Treloar, L.R., 1944. Stress-strain data for vulcanized rubber under various types of deformation. Rubber Chem. Technol. 17 (4), 813–825. https://doi.org/10.1039/TF9444000059.
Treloar, L.R.G., 1975. Physics of Rubber Elasticity. Oxford University Press. ISBN 9780198570271.
Treloar, L.R.G., Riding, G., 1979. A non-Gaussian theory for rubber in biaxial strain. I. Mechanical properties. Proceedings of the Royal Society of London. A. Mathematical and Physical Sciences 369 (1737), 261–280. https://doi.org/10.1098/rspa.1979.0163.
Vernerey, F.J., Long, R., Brighenti, R., 2017. A statistically-based continuum theory for polymers with transient networks. J. Mech. Phys. Solid. 107, 1–20. https://doi.org/10.1016/j.jmps.2017.05.016.
Westbeek, S., van Dommelen, J., Remmers, J., Geers, M., 2018. Multiphysical modelling of the photopolymerization process for additive manufacturing of ceramics. Eur. J. Mech. A Solids 71, 210–223. https://doi.org/10.1016/j.euromechsol.2018.03.020.
Westbeek, S., Remmers, J., van Dommelen, J., Geers, M., 2020. Multi-scale process simulation for additive manufacturing through particle filled vat photopolymerization. Comput. Mater. Sci. 180 https://doi.org/10.1016/j.commatsci.2020.109647.
Wu, J., Zhao, Z., Hamel, C.M., Mu, X., Kuang, X., Guo, Z., Qi, H.J., 2018. Evolution of material properties during free radical photopolymerization. J. Mech. Phys. Solid. 112, 25–49. https://doi.org/10.1016/j.jmps.2017.11.018.
Yamaguchi, K., Nakamoto, T., 1998. Micro fabrication by UV laser photopolymerization. Memoirs of the School of Engineering 50, 33–82. Nagoya University.
Yeoh, O.H., 1990. Characterization of elastic properties of carbon-black-filled rubber vulcanizates. Rubber Chem. Technol. 63, 792–805. https://doi.org/10.5254/1.3538289.
Zakeri, S., Vippola, M., Levänen, E., 2020. A comprehensive review of the photopolymerization of ceramic resins used in stereolithography. Addit. Manuf. 35, 101177 https://doi.org/10.1016/j.addma.2020.101177.
Zarrelli, M., Skordos, A.A., Partridge, I.K., 2010. Toward a constitutive model for cure-dependent modulus of a high temperature epoxy during the cure. Eur. Polym. J. 46, 1705–1712. https://doi.org/10.1016/j.eurpolymj.2010.06.002.